Investigations on a robust profile model for the reconstruction of 2D periodic absorber lines in scatterometry

H. Gross hermann.gross@ptb.de — Physikalisch-Technische Bundesanstalt (PTB), Braunschweig and Berlin, Germany

J. Richter — AMTC GmbH Co.KG, Dresden, Germany

A. Rathsfeld — Weierstrass Institute for Applied Analysis and Stochastics, Berlin, Germany

M. Bär — Physikalisch-Technische Bundesanstalt (PTB), Braunschweig and Berlin, Germany

Scatterometry as a non-imaging indirect optical method in wafer metrology is applicable to lithography masks designed for extreme ultraviolet (EUV) lithography, where light with wavelengths of about 13.5 nm is applied. The main goal is to reconstruct the critical dimensions (CD) of the mask, i.e., profile parameters such as line width, line height, and side-wall angle, from the measured diffracted light pattern and to estimate the associated uncertainties. The numerical simulation of the diffraction process for periodic 2D structures can be realized by the finite element solution of the two-dimensional Helmholtz equation. The inverse problem is expressed as a non-linear operator equation where the operator maps the sought mask parameters to the efficiencies of the diffracted plane wave modes. To solve this operator equation, the deviation of the measured efficiencies from the ones obtained computationally is minimized by a Gauß-Newton type iterative method. In the present paper, the admissibility of rectangular profile models for the evaluations of CD uniformity is studied. More precisely, several sets of typical measurement data are simulated for trapezoidal shaped EUV masks with different mask signatures characterized by various line widths, heights and side-wall angles slightly smaller than 90°. Using these sets, but assuming rectangular structures as the basic profiles of the numerical reconstruction algorithm, approximate line height and width parameters are determined as the critical dimensions of the mask. Finally, the model error due to the simplified shapes is analyzed by checking the deviations of the reconstructed parameters from their nominal values. [DOI: 10.2971/jeos.2010.10053]

Keywords: scatterometry, profile model, critical dimensions (CD), inverse problem

1 INTRODUCTION

As mask and wafer technologies proceed to ever smaller features sizes the demands for a tight control of critical dimensions (CD) on the photo lithographic mask becomes increasingly challenging [1]. Both the feature sizes and the admissible limits of measurement uncertainty decrease continuously. Besides conventional metrology techniques like atomic force, electron and optical microscopy, scatterometry has emerged as an important tool for the characterization of such structures. However, scatterometry [2]–[5] is an indirect optical method working beyond the limit of diffraction and uses far field measurements to reconstruct the sought profile parameters of the mask under inspection. Such an inverse problem in electromagnetism is, from the mathematical point of view, severely ill-posed (see also [6, 7]). Consequently, the determination of the geometrical profile parameters is extremely difficult. Tiny uncertainties in the measurement data usually result in huge errors of the reconstructed structure. Regularization techniques improve the solution of the inverse problems. Nevertheless the accuracy is much less than that of well-posed problems. A better reconstruction is possible only if more a-priori knowledge is used. To cope with this, the class of solutions has to be restricted, i.e., using all available a-priori information together with reasonable model assumptions, the profile geometry must be simplified. Typically, the surface structure is sought in a certain class of gratings described by a finite number of parameters, that are confined to intervals centered around given design values for the mask under investigation.

Figure 1 shows a grating class and its profile model for the cross section over one period of a typical line-space structure for extreme ultraviolet (EUV) lithography, where the wavelength λ is about ~ 13.5 nm. The cross section of the line-space structure is a symmetric polygonal domain composed of three trapezoidal layers of different materials (TaO, TaN, and SiO_2). These trapezoids are defined by the heights p_i, $i = 1, 6, 11$ and by the x-coordinates p_i, $i = 2, 3, 7, 8, 12, 13$ of the corners. Beneath the line-space structure, there are two capping layers of SiO_2 and of Si on top of a $MoSi$ multilayer stack (MLS). The latter stack consists of a periodically repeated group composed of a Mo layer and a Si layer separated by two intermediate layers. Note, that the MLS is added to enable the reflection of EUV waves. Important geometric profile parameters are the height p_6 of the TaN layer (55 - 60 nm) and the x-coordinates p_2 and p_7 of the right corners of the TaN layer. The complex indices of refraction for the involved materials are listed in Table 1 for three wavelengths in the range of 13 nm.

Received July 05, 2010; published September 23, 2010 ISSN 1990-2573

absorber line	n_{λ_1}	k_{λ_1}	n_{λ_2}	k_{λ_2}	n_{λ_3}	k_{λ_3}
TaO	0.94843	0.03100	0.94649	0.03206	0.94456	0.03312
TaN	0.94201	0.03416	0.93917	0.03532	0.93641	0.03657
SiO_2	0.97450	0.01531	0.97348	0.01611	0.97262	0.01681
substrate	n_{λ_1}	k_{λ_1}	n_{λ_2}	k_{λ_2}	n_{λ_3}	k_{λ_3}
Si	0.99967	0.00182	0.99812	0.00184	0.99679	0.00188
MoSi	0.97000	0.00424	0.96660	0.00449	0.96339	0.00476
Mo	0.92552	0.00621	0.92116	0.00677	0.91676	0.00741

TABLE 1 Complex indices of refraction for the involved materials; first three components belong to the absorber line structure and the last three ones to the underlaying capping and multilayer system of the EUV mask; the values at wavelengths $\lambda_1 = 13.389$ nm, $\lambda_2 = 13.664$ nm, and $\lambda_3 = 13.931$ nm are itemized.

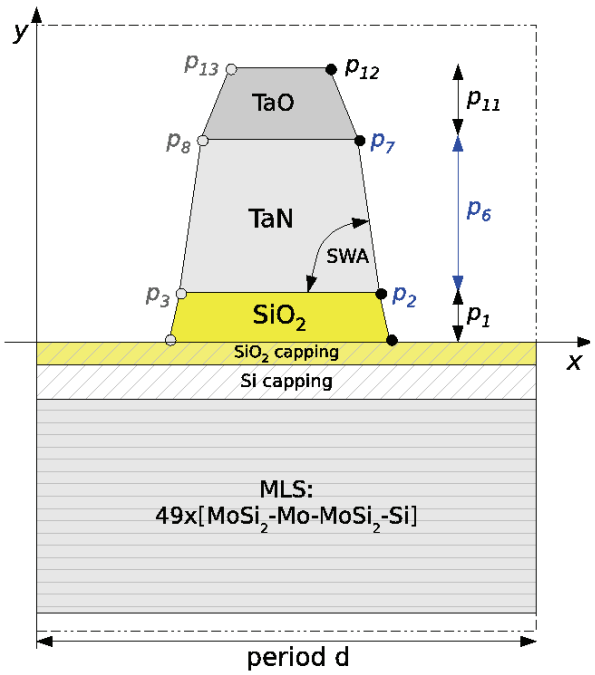

FIG. 1 Scheme of an EUV grating structure including the profile parameters to be reconstructed (in blue).

In the evaluations of EUV measurements described in [8] a symmetric profile is imposed, i.e., the x-coordinates of the corresponding left corners depend on those of the right corners such as $p_3 = d - p_2$ or $p_8 = d - p_7$, where d is the period of the EUV mask. Furthermore the side-wall angle (SWA) for the *TaO* layer was fixed to 82.6°. The cross-section area of this trapezoidal layer is equal to a corresponding *TaO* layer having curved upper edges with a radius of about 6 nm. Additionally, we assumed that the SWA of the SiO_2 layer should be always equal to the SWA of the *TaN* layer above. The latter angle depends on the corners and the height of the *TaN* layer: $\tan(\text{SWA}) = \frac{p_6}{p_2 - p_7}$. We only optimized the three parameters p_2, p_6, and p_7. For all other model parameters, including the heights p_1 (8 nm) and p_{11} (12 nm) of the SiO_2 and the *TaO* layer, the optical indices of the materials, and the widths in the capping or the multilayer system, we suppose constant given values.

The earlier work in [8] investigated the impact of measurement noise and model uncertainties on the uncertainties of the three reconstructed profile parameters. Even for small presumed perturbations (thicknesses of capping layers perturbed by 1% and those of MLS by 0.1%, details in [8]) the standard deviation of the reconstructed side-wall angle is greater than 1.5°. On the other hand, the study revealed that the height of the line-space structure and the line width at middle height of the absorber line are relatively stable with respect to the imposed model-based uncertainties.

In the present investigation we reduce the complexity of the above profile model by imposing a further constraint: All side-wall angles should be equal to 90°. Hence, only the x-coordinate of one of the right corners, say p_2, and the height p_6 of the *TaN* absorber line remain to be reconstructed and the critical dimensions of the mask are approximated only by the height and the width of the absorber stack. To evaluate the admissibility of such a rectangular profile model for the characterization of CD uniformity a comprehensive study is presented: Section 2 recalls some details of the algorithm for the simulation of efficiencies and for the reconstruction of geometry parameters. Measurement sets are simulated for trapezoidal shaped EUV masks with different mask signatures, i.e., with different side-wall angles, line heights and line-to-space ratios (cf. Section 3). For these diffraction patterns, the deviations of the reconstructed profile parameters from the design or nominal values are evaluated applying a rectangle as the basic structure for the reconstruction. The results listed in Section 3.1 show that the reconstruction accuracy achieved with the simple rectangular model is still acceptable in view of varying mask signatures. The stability of the accuracy with respect to measurement noise and noise in the layer stack beneath the line-space structure is discussed in Section 3.2.

2 MODEL OF SCATTEROMETRY

The mathematical basis for modeling the propagation of electromagnetic waves in matter are Maxwell's equations. Their numerical solution represents the direct problem. From the data of the incident light and from characteristic parameters of the irradiated grating, the efficiencies and phase shifts for the different diffraction directions are calculated. The time-harmonic Maxwell equations reduce to the two-dimensional Helmholtz equation if geometry and material properties are invariant in one direction. We use the finite element method (FEM) and truncate the infinite domain of computation to a finite one by coupling with boundary elements (cf. the details in [10, 11]). The FEM solution of this boundary value problem coupled with the so-called Rayleigh expansion provides a general solution above and below the mask for the outgoing

wave modes. Their efficiencies e_j are calculated as the ratio of the incoming energy and the energy radiated into the directions of these wave modes. The indices j of the modes and of the corresponding efficiencies are called the orders of diffraction and are arranged according to the angle of propagation.

The conversion of measured efficiencies into desired geometrical parameters, i.e., the solution of the inverse problem depends crucially on the rigorous modeling by Maxwell's equations and on accurate numerical algorithms. If the sought geometry of the mask is represented by the parameter vector $\mathbf{p} = \{p_n\}$, then the inverse problem can be formulated as an equivalent optimization problem with the following objective functional to be minimized:

$$\Phi(\mathbf{p}) := \sum_{l=1}^{L}\sum_{m=1}^{M}\sum_{j}\omega_j(\lambda_l,\theta_m)\left[e_j(\mathbf{p},\lambda_l,\theta_m) - e_j^{meas}(\lambda_l,\theta_m)\right]^2, \tag{1}$$

where the λ_l, $l = 1,\ldots,L$ are the wavelengths, the θ_m, $m = 1,\ldots,M$ the angles of incidence of the measurement, the $e_j^{meas}(\lambda_l,\theta_m)$ are the measured efficiencies, and the $\omega_j(\lambda_l,\theta_m) > 0$ represent some weight factors. By $e_j(\mathbf{p},\lambda_l,\theta_m)$ we denote the efficiency of order j calculated for wavelength λ_l and angle of incidence θ_m and for a mask geometry defined by the parameters $\mathbf{p}$. If information about the uncertainties of the measured values $e_j^{meas}(\lambda_l,\theta_m)$ is available, then it is common and well accepted for least-square procedures to choose the weight factors as the squared reciprocal uncertainties ($\omega_j(\lambda_l,\theta_m) \propto [u_j(\lambda_l,\theta_m)]^{-2}$). More precisely, we have

$$\Phi(\mathbf{p}) := \sum_{l=1}^{L}\sum_{m=1}^{M}\sum_{j}\frac{1}{[u_j(\lambda_l,\theta_m)]^2}\left[e_j(\mathbf{p},\lambda_l,\theta_m) - e_j^{meas}(\lambda_l,\theta_m)\right]^2 \tag{2}$$

The objective is to find the vector $\mathbf{p}$ that minimizes $\Phi(\mathbf{p})$.

For the following investigations we assume that measurement data, i.e., efficiencies e_j^{meas} for three slightly different wavelengths in the range of 13.5 nm and one angle of incidence $\theta = 6^\circ$ are available. That is, three single incident plane waves and their corresponding diffracted orders are considered. Depending on the ratio of the period of the grating over the wavelength of the incidental light many diffracted orders may exist, but only those will be considered whose efficiencies are significantly greater than the background noise of existing measurement equipments [4, 8]. In compliance with this rule, usually only the orders in the range of -10 to $+10$, i.e., 21 values per wavelength are included in our study. Consequently, the efficiency records have a maximal size of 63 entries and sometimes slightly sparser. To our experience these records are large enough or could be even smaller to get meaningful reconstruction results. In [8] the uncertainty was estimated, and especially the uncertainty $\sigma = 1.5^\circ$, for the reconstructed side-wall angles of EUV masks, was obtained for a medium-sized record of efficiencies composed of overall 25 measured values. In [9] numerical examples for chrome-glass masks inspected with light of wavelength 632.8 nm are given, and basic considerations in regard to sensitivity in dependence on the selected efficiencies and the measurement configurations are discussed.

A FEM based Gauß-Newton type method can be applied to solve the last optimization problem (cf e.g. [12, 13] for details of Gauß-Newton). If the number of measured values is sufficiently large and if the bounds for the sought parameters are chosen appropriately, precise results can be achieved for the inspected masks.

We use the DIPOG software package [14] as the working horse for our investigations. This FEM based Maxwell solver offers a high flexibility including generalized FEM (see also [15]) to compute the highly oscillatory fields typical for EUV scatterometry. Furthermore, optimization methods for many different grating classes are included. In general, the computational costs are high for EUV applications (see below) and investigations for faster simulations such as the reduced basis method [16] could be very helpful.

3 SIMPLIFIED PROFILE MODEL

To evaluate the admissibility of a rectangular profile model in dependence on varying mask signature, first the light diffraction efficiencies of different trapezoidal shaped EUV masks are calculated by generalized FEM with a very high level of discretization, i.e., with a very fine grid of triangles in the domain of computation spreading over one period (cf. [14]). As mentioned above, these simulations are done for three plane waves with slightly different wavelengths $\lambda_1 = 13.389$ nm, $\lambda_2 = 13.664$ nm, $\lambda_3 = 13.931$ nm and the same angle of incidence $\theta = 6^\circ$. The efficiencies are calculated with the GFEM algorithm of DIPOG at a high error level to reach 0.01% accuracy, and over a triangulation different from those used in the reconstruction algorithm. On a Linux workstation with four Intel Xeon processors (X5460 @ 3.16 GHz) the computation for such a simulation takes about 75 minutes.

In Figure 2 the trapezoidal shaped mask profiles used for simulating measured data are depicted as blue lines. By contrast to Figure 1 and the associated investigations in [8], each layer of the absorber stack has the same side-wall angle. The corresponding geometrical parameters characterizing different mask signatures are given in Table 2. From all possible combinations of the entries, two groups each with 25 profiles are chosen: The first, (L:S) $\otimes$ (SWA), contains all combinations with the height of the *TaN* layer fixed to 57.5 nm and the second, (L:S) $\otimes$ (hTaN), all combinations with side-wall angle fixed to 85°. The simulated diffraction efficiencies in these groups are taken as "measured" data for the profile reconstructions, but only those efficiencies are included into the data sets whose values e_j^{meas} are greater than $5 \cdot 10^{-5}$. This ensures that the values are significantly larger than the background noise (cf. Section 3.2).

3.1 Impact of different mask signatures

The objective of this study is to examine the mismatch of the reconstructed widths and heights in dependence on different mask signatures described by different line-to-space ratios, heights, and side-wall angles of the absorber line, respectively. For each reconstruction of a specific mask, an optimization (cf. Section 2) has been performed, i.e., the objective functional

Parameter					
hTaN /nm	53.5	55.5	57.5	59.5	61.5
L:S	1:11	1:5	1:2	1:1	2:1
(= CD/(d-CD)	70/(840-70)	140/(840-140)	140/(420-140)	280/(560-280)	280/(420-280)
SWA /°	83	84	85	86	87

TABLE 2 Specific parameters used for the simulated diffraction patterns: hTaN as height of the TaN layer, L:S as the line-to-space ratios and SWA as the side-wall angle for all absorber layers; here CD denotes the bottom line width and d the period in nm.

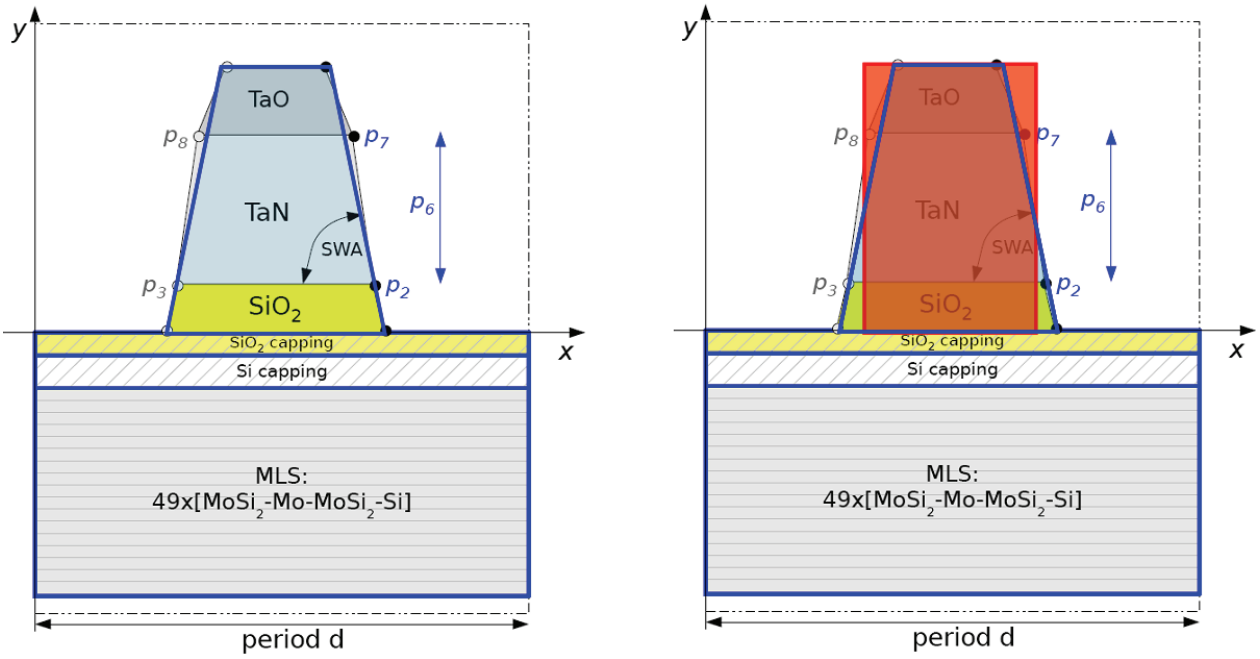

FIG. 2 Left: Scheme of trapezoidal EUV line-space structure used for simulating diffraction patterns; Right: EUV scheme overlayed with a (red) rectangular profile which is used for the reconstruction of line width and height.

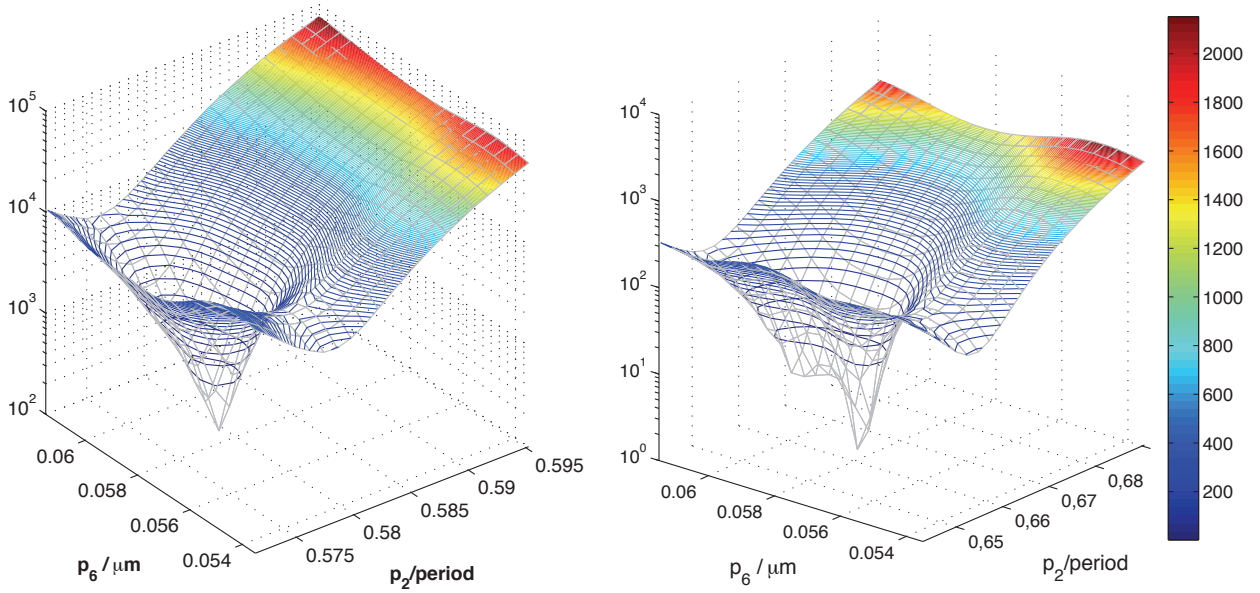

FIG. 3 Functional $\Phi(\mathbf{p})$ defined by Eq. (2) for two different signatures: SWA = 83°, L:S = 1:5 (line width = 140 nm & period = 840 nm) (left) and SWA = 85°, L:S = 1:2 (line width = 140 nm & period = 420 nm) (right); height of TaN layer in both cases is 57.5 nm

$\Phi(\mathbf{p})$ has been minimized. Figure 3 shows two examples of Φ. In the selected range of the parameters a well defined minimum can be recognized. Clearly, there will be systematic deviations of the reconstructed values from the nominal values for the trapezoids included in the input data. Their distribution over varying mask signatures has to be quantified in order to accept or reject the application of a rectangular profile reconstruction for the estimation of CD uniformity.

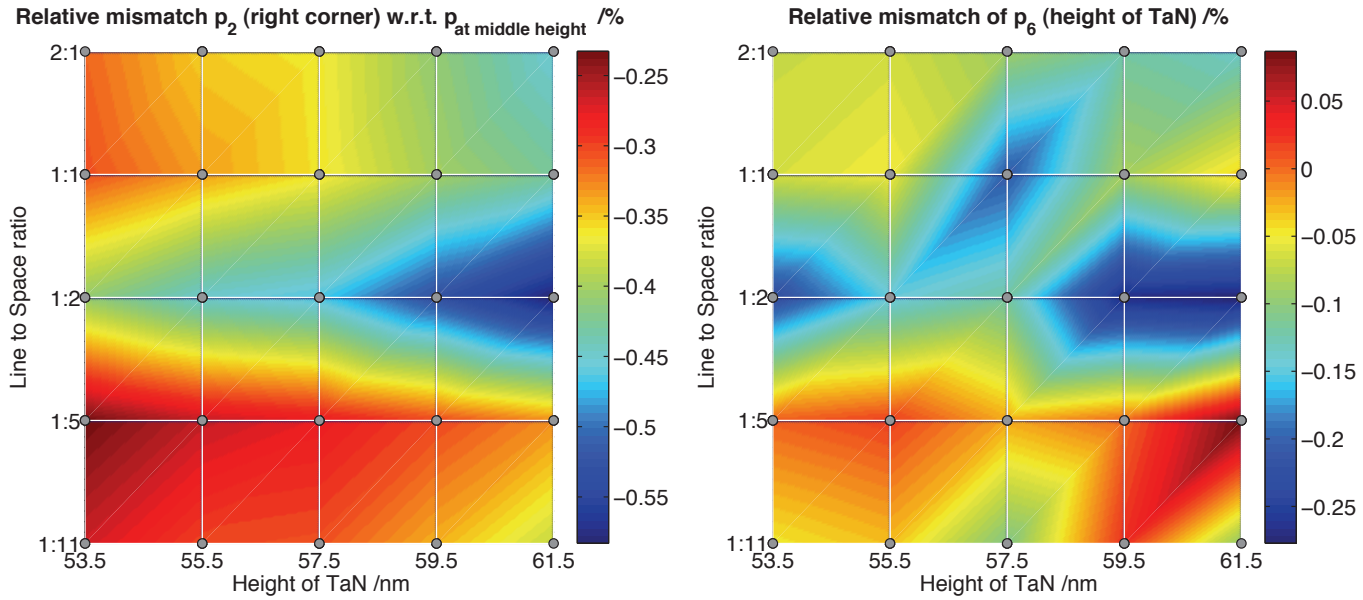

FIG. 4 Distribution of relative deviations for the reconstructed right corner point p_2 (left) and the reconstructed height of the TaN layer p_6 (right) for 25 different combinations of line-to-space ratio and height of the absorber line; variations are depicted as a temperature map with interpolated colors in between the evaluation points; the side-wall angle was fixed to 85° for all examined combinations.

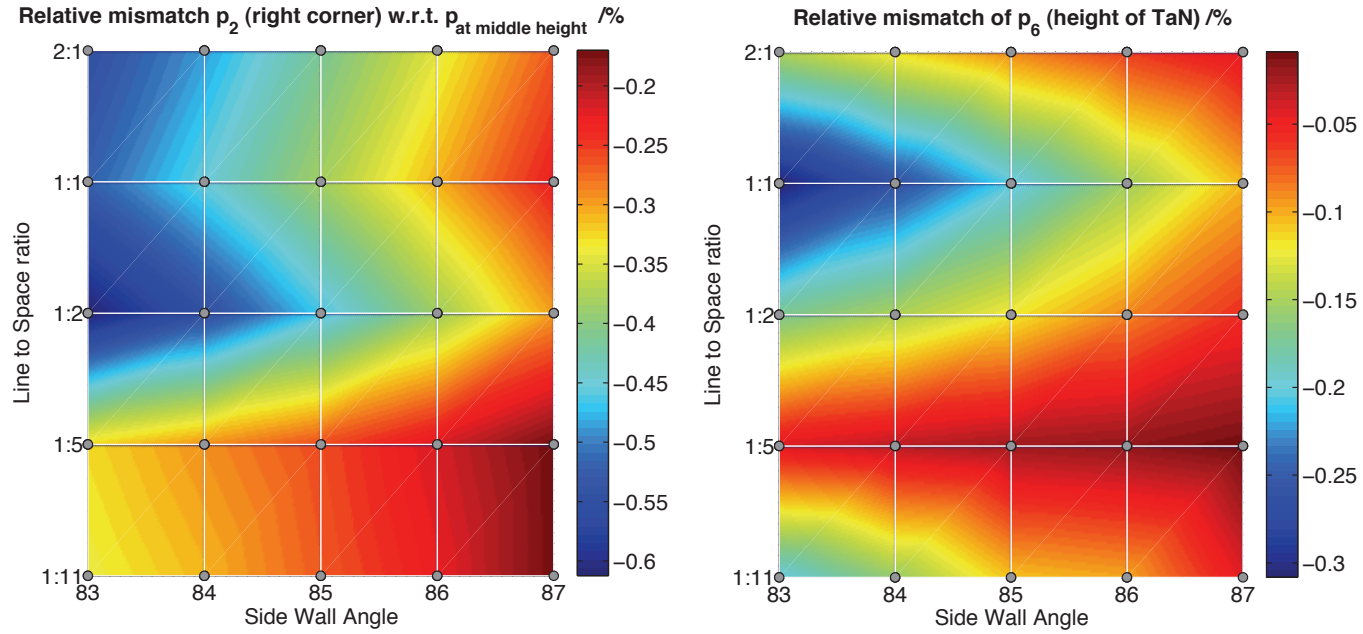

FIG. 5 Distribution of relative deviations for the reconstructed right corner point p_2 (left) and the reconstructed height of the TaN layer p_6 (right) for 25 different combinations of line-to-space ratio and side-wall angles of the absorber line; variations are depicted as a temperature map with interpolated colors in between the evaluation points; the height of the TaN layer was fixed to 57.5 nm for all examined combinations.

The resulting deviations of the reconstructed parameters p_2 and p_6 are shown for the group of masks (L:S) $\otimes$ (hTaN) in Figure 4 and for (L:S) $\otimes$ (SWA) in Figure 5. The variations are depicted as a temperature map with interpolated colors in between the evaluation points. Relative deviations with respect to the nominal values are given. For the reconstructed right corner p_2, the x-coordinate at the middle of the trapezoid is used as the reference value.

We recognize systematic shifts in the reconstructed profile parameters to slightly smaller values. However, for all evaluated signatures, the modulus of the relative deviation is always smaller than 0.6% for the reconstructed right corner and 0.3% for the reconstructed height of the TaN absorber layer. Furthermore we recognize that the modulus of all relative deviations decreases with increasing side-wall angle as was expected (cf. Figure 5). In Figure 6 these results are depicted as statistical boxplots.

3.2 Impact of detector noise and multilayer perturbations

In order to study, how sensible the mismatch of the robust rectangular profile model is in dependence on measurement

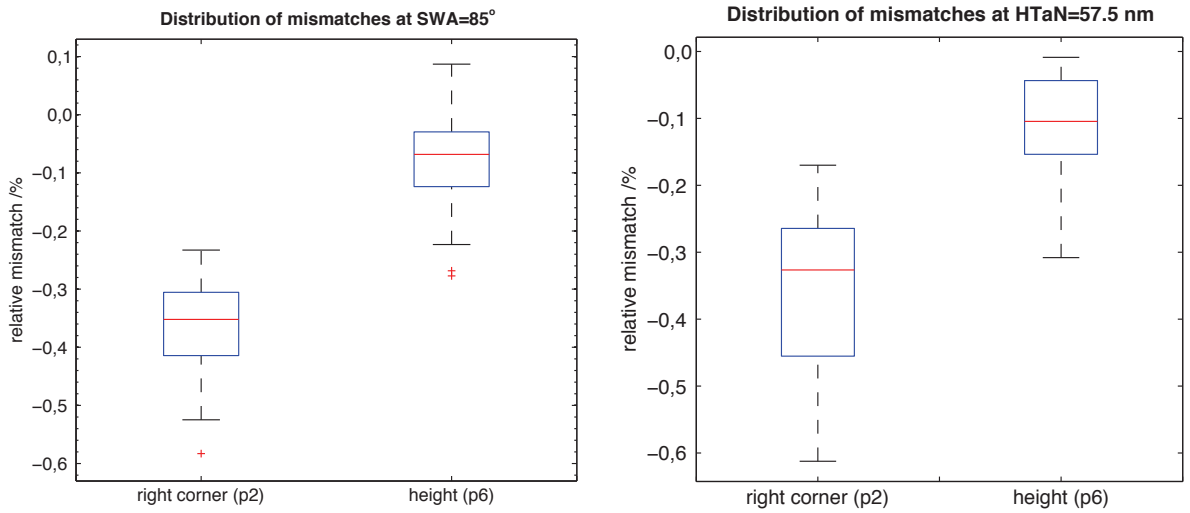

FIG. 6 Distribution of relative deviations for a fixed side-wall angle of 85° (left) and for a fixed absorber height of 57.5 nm (right) shown as statistical boxplots. They contain the lower and upper quartiles as blue boxes, the median as red lines and the extreme values as whiskers. Outliers are depicted as red plus signs.

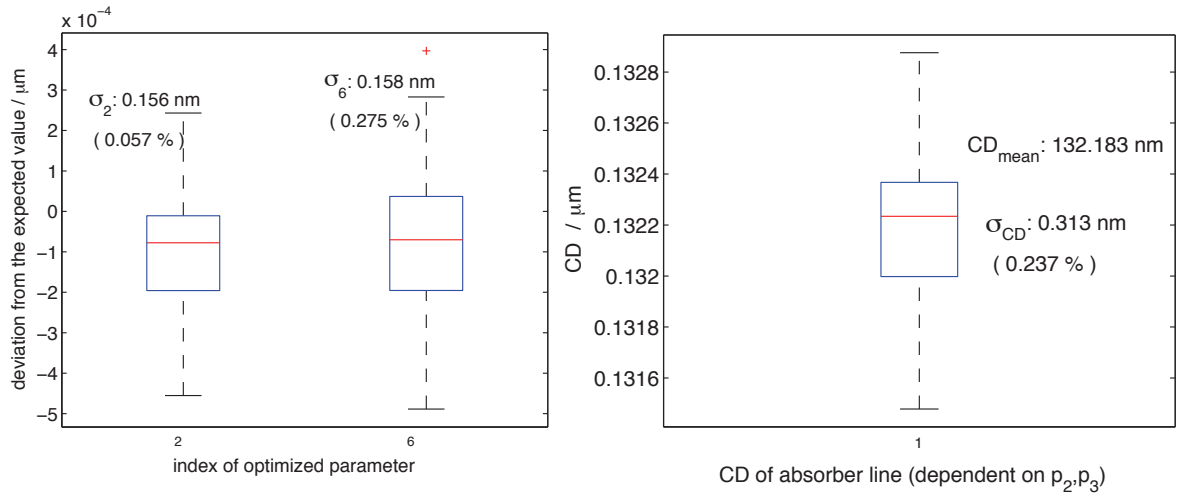

FIG. 7 Impact of disturbed efficiencies (3% rel.noise & 0.001% background noise) and disturbed widths of capping/multilayer system (1%/0.1%) on the reconstructed values p_2, p_6 and CD (line width) of a rectangular profile model calculated by Monte Carlo.

noise and thickness variations in the capping and the multilayer system, the following noise experiment has been performed: For one of the examined signatures (L:S = 1 : 2 & hTaN = 57.5 nm & SWA = 85°), we have applied a Monte Carlo (MC) simulation in the spirit of the recommendations in Supplement 1 of the GUM [17], i.e., complete profile reconstructions have been repeated many times with randomly perturbed measurement data and simultaneously perturbed widths of capping and multilayer system. The uncertainties of the input data for the numerical reconstruction algorithm generate uncertainties of the reconstructed profile parameters, and the statistics of the deviation from the expected values of the undisturbed case has been derived. Alternative approaches assessing the uncertainties are proposed by Al-Assad and Byrne [13] or Germer *et al* [18].

According to measurement experience with the EUV spectroscopic reflectometer (see [8] for more details), the measured efficiency values e_j^{meas} are normally distributed and their variance can be supposed to be of the sum of the variances of two independent random variables

$$u_j^2 = (a \cdot e_j^{meas})^2 + b_g^2, \tag{3}$$

where $a \cdot e_j^{meas}$ indicates noise proportional to e_j^{meas} with a constant factor a in the range of 0.01–0.03 for real EUV measurements. Power fluctuations of the incidental beam during the recording of the diffraction patterns are the main reason to consider values of $a > 0$. The mean time to record an EUV diffraction pattern is about one hour. For the MC simulation, we have assumed $a = 0.03$. In the second term b_g qualifies the background noise of the spectroscopic reflectometer of about $1 \cdot 10^{-5}$ (equivalent to 0.001%, if the efficiencies are given in per cent). For the noise in the width of the capping/MLS models, we have assumed normal distributions with zero mean and standard deviations of 1% for the two capping layer widths and 0.1% for the thicknesses in the *MoSi* multilayer system.

The resulting deviations of the reconstructed profile parameters p_2, p_6 for this MC simulation and the corresponding deviations of the line width are given in Figure 7 as boxplots. As

compared to the relative deviations caused by the rectangular profile model (cf. Figure 5), the impact of the examined measurement noise (3% relative noise/0.001% background noise) and the imposed thickness perturbations (1% capping/0.1% MLS) is small for the right corner p_2 and in the same range for the height p_6 of the *TaN* absorber line. The last is not surprising because the imposed thickness variations are affecting the reflectance of the EUV grating significantly (cf. [8] for more details).

4 SUMMARY

We have numerically reconstructed the height and the line-width uniformity of absorber lines in 2D line-space structures for EUV lithography. Although the determination of the side-wall angle of trapezoidal cross sections is extremely sensitive with respect to model errors and measurement uncertainties (cf. [8]), the computation of height and line width is quite robust. Assuming side-wall angles as low as 83°, we have demonstrated that even a simplified rectangular model for the cross section of the absorber line is sufficient for the reconstruction of height and line width with reasonable accuracy. Moreover, this rectangular reconstruction is stable with respect to typical measurement uncertainties and perturbations in the thicknesses of the multilayer system beneath the line-space structure validating its admissibility under more relasitic conditions. Of course, there are further impacts of model imperfections such as line-edge roughness (LER) and line-width roughness (LWR), respectively, and first investigations [19] of their effects on the reconstructed line profiles are confirming the robustness of the rectangular reconstruction.

ACKNOWLEDGEMENTS

The presented investigations are part of the project CDuR32 funded by the German Federal Ministry of Eduction and Research (BMBF).

References

[1] ITRS *International Technology Roadmap for Semiconductors, 2005 Edition, Lithography* http://www.itrs.net/Links/2005ITRS/Litho2005.pdf

[2] M. Wurm, B. Bodermann, and W. Mirandé, "Evaluation of scatterometry tools for critical dimension metrology" DGaO Proc. **106**, (2005).

[3] H. Gross, R. Model, M. Bär, M. Wurm, B. Bodermann, and A. Rathsfeld, "Mathematical modelling of indirect measurements in scatterometry" Measurement **39**, 782–794 (2006).

[4] J. Perlich, F.-M. Kamm, J. Rau, F. Scholze, and G. Ulm, "Characterization of extreme ultraviolet masks by extreme ultraviolet scatterometry" J. Vac. Sci. Technol. **B22**, 3059–3062 (2004).

[5] J. Pomplun, S. Burger, F. Schmidt, F. Scholze, C. Laubis, and U. Dersch, "Finite element analysis of EUV scatterometry" Proc. SPIE **6617**, 18–21 (2007).

[6] D. Colton, and R. Kress, *Inverse Acoustic and Electromagnetic Scattering Theory* (Second Edition, Springer-Verlag, New York 1998).

[7] J. Elschner, and M. Yamamoto, "An inverse problem in periodic diffractive optics: Reconstruction of Lipschitz grating profiles" Appl. Anal. **81**, 1307–1328 (2002).

[8] H. Gross, A. Rathsfeld, F. Scholze, and M. Bär, "Profile reconstruction in extreme ultraviolet (EUV) scatterometry: modeling and uncertainty estimates" Meas. Sci.Technol. **20**, 105102 (2009).

[9] H. Gross, and A. Rathsfeld, "Sensitivity analysis for indirect measurement in scatterometry and the reconstruction of periodic grating structures" Wave. Random Complex **18**, 129–149 (2008).

[10] J. Elschner, R. Hinder, and G. Schmidt, "Finite element solution of conical diffraction problems" Adv. Comput. Math. **16**, 139–156 (2002).

[11] G. Bao, "Finite element approximation of time harmonic waves in periodic structures" SIAM J. Numer. Anal. **32**, 1155–69 (1995).

[12] J. Nocedal, and S. J. Wright, *Numerical optimization* (Springer Verlag, New-York, 2000).

[13] R. M. Alassaad, and D. M. Byrne, "Error Analysis in Inverse Scatterometry I: Modeling" J. Opt. Soc. Am. A **24**, 326–338 (2007).

[14] *DIPOG Homepage* http://www.wias-berlin.de/software/DIPOG

[15] O. Cessenat, and B. Depres, "Application of an ultra weak variational formulation of elliptic PDEs to the two-dimensional Helmholtz problem" SIAM J. Numer. Anal. **35**, 255–299 (1998).

[16] J. Pomplun, and F. Schmidt, "Reduced basis method for fast and robust simulation of electromagnetic scattering problems" Proc. SPIE **7390**, 73900I (2009).

[17] Joint Committee for Guides in Metrology BIPM, IEC, IFCC, ILAC, ISO, IUPAC, IUPAP, and OIML, "Evaluation of measurement data – Supplement 1" in *Guide to the expression of uncertainty in measurement - Propagation of distributions using a Monte Carlo method* (Bureau International des Poids et Mesures JCGM 101, 2008).

[18] T. A. Germer, H. J. Patrick, R. M. Silver, and B. Bunday, "Developing an uncertainty analysis for optical scatterometry" Proc. SPIE **7272**, 72720T (2009).

[19] A. Kato, and F. Scholze, "The effect of line roughness on the reconstruction of line profiles for EUV masks from EUV scatterometry" Proc. SPIE **7636**, 76362I (2010).